Proceedings of the Sixth International Conference on
Railway Technology: Research, Development and Maintenance
Edited by: J. Pombo
Civil-Comp Conferences, Volume 7, Paper 12.1
Civil-Comp Press, Edinburgh, United Kingdom, 2024
ISSN: 2753-3239, doi: 10.4203/ccc.7.12.1

Energy Harvesting in High-Speed Railway Bridges Using Magnetoelastic Materials

J. C. Cámara-Molina,[1] A. Romero,[1] P. Galvín,[1] P. Marín,[2,3] M. D. Martínez-Rodrigo[4] and E. Moliner[4]

[1] **Escuela Técnica Superior de Ingeniería, Universidad de Sevilla Spain**
[2] **Instituto de Magnetismo Aplicado, UCM-ADIF Las Rozas, Spain**
[3] **Departamento de Física de Materiales, Universidad Complutense de Madrid (UCM) Spain**
[4] **Department of Mechanical Engineering and Construction, Universitat Jaume I Castellon, Spain**

Abstract

This paper explores energy harvesting from vibrations induced by train passages in High-Speed railway bridges using magnetoelastic material (MsM). This research proposes an analytical approach derived from a variational formulation to obtain the governing equations of MsM. Moreover, an optimal design procedure is considered to produce the maximum power. Finally, the proposed model is verified in a case study using experimental records of a railway bridge under operating conditions. The conclusions drawn from the experimental case study show that the harvested energy in the train passage could be E=5.28 mJ. The results of this analysis could be helpful for low power consumption devices, nodes, and sensors of monitoring systems in remote areas, and also for the development of harvesters as direct structural health monitoring devices.

Keywords: magnetoelasticity, energy harvesting, railway bridges, high-speed train, tuning frequency, optimal design, additive manufacturing, genetic algorithm.

1 Introduction

In recent years, the successful implementation of IoT for real-time Structural Health Monitoring (SHM) in buildings and civil engineering infrastructures has supported advances in predictive maintenance strategies. These innovations enable the assessment of rail system serviceability conditions without disrupting traffic and at reduced costs. Despite these achievements, one of the most limiting factors in the implementation of these monitoring systems is the need for a reliable power supply. Lack of access and maintenance operations in remote areas can limit their practical implementation [1].

To address the power supply challenge, an alternative approach involves energy harvesting from ambient vibrations, providing a sustainable solution for sensors and nodes in monitoring systems. Electromagnetic, electrostatic, and piezoelectric energy harvesting methods are commonly used to convert vibration energy into electricity. Although piezoelectric mechanisms are widely used due to their compatibility with Micro-Electro-Mechanical Systems (MEMS), they come with certain limitations, such as ageing, depolarisation, and brittleness [2]. This paper studies energy harvesting from vibrations induced by train passages in railway bridges using magnetoelastic material (MsM). Magnetoelastic materials take advantage of the Villari effect to generate energy from vibrations, inducing a change in material magnetisation upon deformation. This change is harnessed to produce electrical energy through Faraday's law in a pick-up coil.

This research presents an approach derived from a variational formulation to obtain the governing equations of magnetoelastic energy harvesting systems. The harvester configuration is a unimorph cantilever beam with a tip mass. An optimal design procedure is considered to maximise the output power. Finally, the proposed model is verified in a case study using experimental records of a railway bridge under operating conditions.

2 Formulation and analysis approach

The proposed approach considers an energy harvesting device attached to the bridge at the coordinate x_b (see Figure 1). This device is subjected to the vertical vibrations of the bridge, denoted as $z_b(x_b, t)$, induced by the railway traffic. The dynamic behaviour of the device is described by a coupled magnetoelastic-mechanical model. The energy harvester comprises a unimorph cantilever beam with a tip mass M_t (see Figure 1). The system includes a perfectly attached magnetostrictive patch to the substructure and a pick-up coil, and is connected to an electrical load. The dimensions of the beam are length L_s, width b_s and thickness h_s, while the dimensions of the magnetoelastic plate are length L_p, width b_p and thickness h_p. The properties of the substructure material are defined by Young's modulus E_s and the mass density ρ_s.

The unimorph beam has two different sections: i) the part with MsM given by the longitudinal coordinate $x \leq L_p$; and ii) the remaining part of the substructure defined

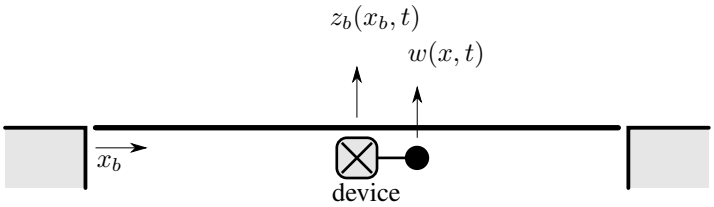

Figure 1: Scheme of bridge/harvester system [3].

by $L_p \leq x \leq L_s$. The following dimensionless parameters relate the geometry, mass, and bending stiffness of both parts:

$$\beta = \frac{L_p}{L_s}, \qquad \gamma = \frac{\overline{EI}}{E_s I_s}, \qquad \tau = \frac{\overline{m}}{\rho_s h_s b_s} \tag{1}$$

where $E_s I_s$ and $\rho_s h_s b_s$ are the bending stiffness and mass per unit length of the substructure; and $\overline{EI}$ and $\overline{m}$ are the equivalent bending stiffness and mass per unit length of the beam section with MsM. Hence, β, γ and τ relate the length, bending stiffness, and mass per unit length of the section with MsM to the substructure, respectively, and are bounded to $\beta \leq 1$, $\gamma > 1$ and $\tau > 1$.

The constitutive equations of the MsM are [4]:

$$\begin{Bmatrix} \mathbf{T} \\ \mathbf{B} \end{Bmatrix} = \begin{bmatrix} \mathbf{c}^H & -\mathbf{e} \\ \mathbf{e} & \boldsymbol{\mu}^S \end{bmatrix} \begin{Bmatrix} \mathbf{S} \\ \mathbf{H} \end{Bmatrix} \tag{2}$$

Where $\mathbf{T}$ is the stress vector, $\mathbf{B}$ is the magnetic flux density vector, $\mathbf{S}$ is the elastic strain vector, $\mathbf{H}$ is the magnetic field intensity vector, $\mathbf{c}^H$ is the elastic stiffness matrix evaluated in a constant magnetic field, $\mathbf{e}$ is the magnetomechanical coefficient, and μ is the absolute permeability at constant strain.

According to the Euler-Bernoulli assumptions, the shear deformation and rotary inertia of the unimorph beam may be neglected. The vertical displacement of the tip mass produces longitudinal stress in the MsM patch. The axial strain and magnetisation are assumed both in the longitudinal direction 3, and therefore the device operates in the 33 mode. Then Equations (2) can be reduced to the following:

$$T_3(x,z,t) = c_{33}^H S_3(x,z,t) - e_{33} H_3(x,z,t) \tag{3}$$

$$B_3(x,z,t) = e_{33} S_3(x,z,t) + \mu_{33}^S H_3(x,z,t) \tag{4}$$

where the elastic stiffness component c_{33}^H represents the Young's modulus of the MsM, e_{33} is the magnetomechanical constant, μ_{33}^S is the absolute permeability at constant strain, z is the vertical coordinate of the beam section and t stands for the time.

The coupled magnetomechanical behaviour of the bimorph beam is described by the governing equations (3) and (4). Magnetisation $H_3(t)$ is expressed by Ampère's

law with the assumption of a long and thin solenoid coil:

$$H_3(t) = \frac{Ni(t)}{L_p} \tag{5}$$

where N is the number of turns of the pick-up coil and $i(t)$ is the induced electric current. It is assumed that the magnetic field intensity does not depend on the longitudinal coordinate x, and the patches are thin enough to neglect their contribution to the bending stiffness.

Furthermore, the axial deformation in the MsM patch S_3 is due to bending and is defined according to the Euler-Bernoulli assumption:

$$S_3(x, z, t) = -z\frac{\partial^2 w(x,t)}{\partial x^2} \tag{6}$$

Similarly, the longitudinal deformation in the substructure becomes $\varepsilon_x = -z\partial^2 w/\partial x^2$.

The equilibrium equation of the cantilever beam subjected to base excitation is [3]:

$$\frac{\partial^2 M(x,t)}{\partial x^2} + m(x)\frac{\partial^2 w(x,t)}{\partial t^2} = -\left[m(x) + M_t\delta(x - L_s)\right]\frac{\partial^2 z_b(x_b,t)}{\partial t^2} \tag{7}$$

where $\delta(x)$ is the Dirac delta function and $m(x)$ represents the mass per unit length of the beam. The mass per unit length is $m(x) = \rho_s h_s b_s$ ($L_p \leq x \leq L_s$), while the mass of the beam section with MsM is defined by the parameter τ according to Equation (1) as $m(x) = \tau\rho_s h_s b_s$ ($0 \leq x \leq L_p$). The mass M_t is assumed to be a point mass. The effect of viscous damping has been omitted in the equilibrium equation for simplicity, and will be later introduced in the governing equation in the following section.

The bending moment of the beam section with MsM is given by:

$$M(x,t) = -b_p\left[\int_{-h_c}^{h_s-h_c} z\sigma_x(x,z,t)\,dz + \int_{h_s-h_c}^{h_s+h_p-h_c} zT_3(x,z,t)\,dz\right], \qquad 0 \leq x \leq L_p \tag{8}$$

where σ_x represents the longitudinal stress in the substructure ($\sigma_x = E_s\varepsilon_x$), and h_c is the distance from the bottom of the substructure to the neutral axis. The expression of the bending moment is further elaborated according to Equations (3) and (6) as:

$$\begin{aligned} M(x,t) = b_p\Bigg[&\int_{-h_c}^{h_s-h_c} z^2 E_s\frac{\partial^2 w(x,t)}{\partial x^2}\,dz + \\ &\int_{h_s-h_c}^{h_s+h_p-h_c}\left(z^2 c_{33}^H\frac{\partial^2 w(x,t)}{\partial x^2} + ze_{33}H_3(x,z,t)\right)dz\Bigg] \end{aligned} \tag{9}$$

Thus, the bending moment is obtained after integration:

$$M(x,t) = \gamma E_s I_s\frac{\partial^2 w(x,t)}{\partial x^2} + \frac{Ne_{33}h_{pc}b_p h_p}{L_p}i(t), \qquad 0 \leq x \leq L_p \tag{10}$$

where $h_{pc} = (2h_s + h_p - 2h_c)/2$ is the distance from the neutral axis of the beam to the centre line of the magnetoelastic patch. The parameter γ relates the bending stiffness of the beam section with the MsM to the bending stiffness of the substructure:

$$\gamma = \frac{h_s^4 + 2h_p h_s \left(2h_p^2 + 3h_p h_s + 2h_s^2\right) n + h_p^4 n^2}{h_s^3 \left(h_s + h_p n\right)} \tag{11}$$

where $n = c_{33}^H / E_s$.

The bending moment of the substructure is $M(x,t) = E_s I_s \partial^2 w(x,t)/\partial x^2, \quad L_p \leq x \leq L_s$.

2.1 Governing equations

The equation of motion of the unimorph beam is derived from Hamilton's principle, expressing the kinetic energy E_k, the potential energy E_p, and the virtual work δW performed by the base excitation in terms of the generalised coordinate $q(t)$. The beam deflection is approximated by:

$$w(x,t) = q(t)\psi(x) \tag{12}$$

where the generalised coordinate $q(t)$ represents the tip displacement and $\psi(x)$ is a dimensionless shape function that satisfies the boundary conditions. Then, the Lagrange equation of motion is written as follows:

$$\frac{d}{dt}\left(\frac{\partial E_k}{\partial \dot{q}}\right) - \frac{\partial E_k}{\partial q} + \frac{\partial E_p}{\partial q} = Q \tag{13}$$

where the virtual work is expressed as $\delta W = Q\delta q$.

The dimensionless shape function $\psi(x)$ can be estimated from the static equilibrium (Equation (7)) of a beam under a unit tip load. Clamped boundary condition at the fixed end and compatibility of displacement and rotation at $x = L_p$ are impossed.

The constitutive equations (3) and (4) expressed in the generalised coordinates are obtained by combining Equations (6) and (12):

$$T_3(x,z,t) = -c_{33}^H z \frac{\partial^2 \psi(x)}{\partial x^2} q(t) - \frac{N e_{33}}{L_p} i(t) \tag{14}$$

$$B_3(x,z,t) = -e_{33} z \frac{\partial^2 \psi(x)}{\partial x^2} q(t) + \frac{N \mu_{33}^S}{L_p} i(t) \tag{15}$$

The kinetic energy E_k, the strain energy E_d and the magnetic energy E_m are defined as:

$$E_k = \frac{1}{2}\left[\int_{\Omega_s} \rho_s \dot{w}(x,t)\dot{w}(x,t)\,d\Omega + \int_{\Omega_p} \rho_p \dot{w}(x,t)\dot{w}(x,t)\,d\Omega + M_t \dot{w}(L_s,t)^2\right] \quad (16)$$

$$E_d = \frac{1}{2}\left[\int_{\Omega_p} T_3(x,z,t)S_3(x,z,t)\,d\Omega + \int_{\Omega_s} \sigma_x(x,z,t)\varepsilon_x(x,z,t)\,d\Omega\right] \quad (17)$$

$$E_m = -\frac{1}{2}\int_{\Omega_p} B_3(x,z,t)H_3(x,z,t)\,d\Omega \quad (18)$$

Then, the potential energy is calculated from the strain and magnetic energies as:

$$E_p = E_d + E_m \quad (19)$$

The virtual work of the external forces $\delta W_{ext} = Q\delta q$ is expressed in terms of effective mass as $\delta W_{ext} = -M_{eff}\ddot{z}(x_b,t)\delta q$.

Finally, the Lagrange equation of motion (Equation (13)) becomes:

$$M_{eq}\ddot{q}(t) + K_{eq}q(t) + Gi(t) = -M_{eff}\ddot{z}_b(x_b,t) \quad (20)$$

where the equivalent mass and stiffness, M_{eq} and K_{eq}, the effective mass M_{eff} and the magnetomechanical coupling coefficient G are given by:

$$M_{eq} = \int_0^{L_p} \tau\rho_s h_s b_s \psi(x)^2\,dx + \int_{L_p}^{L_s} \rho_s h_s b_s \psi(x)^2\,dx + M_t \quad (21)$$

$$M_{eff} = \int_0^{L_p} \tau\rho_s h_s b_s \psi(x)\,dx + \int_{L_p}^{L_s} \rho_s h_s b_s \psi(x)\,dx + M_t \quad (22)$$

$$K_{eq} = \int_0^{L_p} \gamma E_s I_s \left(\frac{\partial^2\psi(x)}{\partial x^2}\right)^2 dx + \int_{L_p}^{L_s} E_s I_s \left(\frac{\partial^2\psi(x)}{\partial x^2}\right)^2 dx \quad (23)$$

$$G = \int_0^{L_p} \frac{N e_{33} h_{pc} A_m}{L_p}\frac{\partial^2\psi(x)}{\partial x^2}\,dx \quad (24)$$

with $A_m = h_p b_p$ the area of the MsM.

The Villari effect relates changes in the material magnetisation due to the strain. The magnetic field induces a voltage $v(t)$ in a pick-up coil according to Faraday's law. Thus, the voltage is obtained according to Equation (15) from:

$$\frac{dv(t)}{dx}dx = \frac{d}{dx}\left(-N\frac{d}{dt}\int_{A_m} B_3(x,z,t)\,dA\right)dx \quad (25)$$

Substituting Equation (15) into Equation (25) and integrating, the voltage across the coil becomes:

$$v(t) = \frac{N h_p b_p e_{33} h_{pc}}{L_p}\int_0^{L_p} \frac{\partial^2\psi(x)}{\partial x^2}\,dx\dot{q}(t) - \frac{N^2 h_p b_p \mu_{33}^S}{L_p}\dot{i}(t) \quad (26)$$

Moreover, the following expression is derived considering the magnetomechanical coupling coefficient (Equation 24) and the internal resistance of the coil NR_c (R_c is the resistance of one turn):

$$v(t) = G\dot{q}(t) - L\dot{i}(t) - NR_c i(t) \tag{27}$$

where L is the equivalent inductance of the coil:

$$L = \frac{N^2 \mu_{33}^S A_m}{L_p} \tag{28}$$

The system is connected to a load resistance R_l to estimate the electrical energy generated by the harvester. Then, the coupled electromechanical governing equation is obtained from Equation (27) considering that the voltage across the load resistance equals the induced voltage. Thus, the voltage can be expressed as $v(t) = R_l i(t)$ and the coupled electromechanical governing equation is:

$$G\dot{q}(t) - L\dot{i}(t) - NR_c i(t) - R_l i(t) = 0 \tag{29}$$

Furthermore, an equivalent damping is considered in the system. The damping is introduced in Equation (20) to represent the dissipation of mechanical energy due to the viscous effects of the harvester. The equivalent damping is defined by the damping coefficient $C_{eq} = 2\zeta\omega M_{eq}$ where ζ represents the mechanical damping ratio and $\omega = \sqrt{K_{eq}/M_{eq}}$ is the natural frequency of the device. Consequently, the governing equations of the problem are derived from equations (20) and (29) considering the effect of the equivalent damping and dividing by the equivalent mass of the system:

$$\ddot{q}(t) + 2\zeta\omega\dot{q}(t) + \omega^2 q(t) + \frac{G}{M_{eq}} i(t) = -\frac{M_{eff}}{M_{eq}} \ddot{z}_b(x_b, t) \tag{30}$$

$$L\dot{i}(t) + (R_l + NR_c) i(t) - G\dot{q}(t) = 0 \tag{31}$$

The governing equations represent the magnetoelectromechanical behaviour of the simplified lumped mass model in Figure 2. The lumped-parameter model is represented by the generalised coordinate $q(t)$ and the electric current $i(t)$. The coupling terms in Equations (30) and (31) represent an equivalent gyrator that relates the time derivative of the generalised coordinate to the electric current. The magnetomechanical coefficient G can be considered as the gyration resistance.

The governing equations can be evaluated in terms of amplitude and phase, assuming a harmonic base excitation of the form $z_b(x_b, t) = z_0(x_b, \overline{\omega}) \exp(\iota\overline{\omega}t)$:

$$(-\overline{\omega}^2 + 2\iota\overline{\omega}\zeta\omega + \omega^2) q_0(\overline{\omega}) + \frac{G}{M_{eq}} i_0(\overline{\omega}) = \frac{M_{eff}}{M_{eq}} \overline{\omega}^2 z_0(x_b, \overline{\omega}) \tag{32}$$

$$(\iota\overline{\omega}L + NR_c + R_l)\, i_0(\overline{\omega}) - \iota\overline{\omega} G q_0(\overline{\omega}) = 0 \tag{33}$$

where $\overline{\omega}$ is the frequency of excitation and the imaginary unit number is denoted by the Greek letter ι to avoid confusion with the induced current. The solution of the

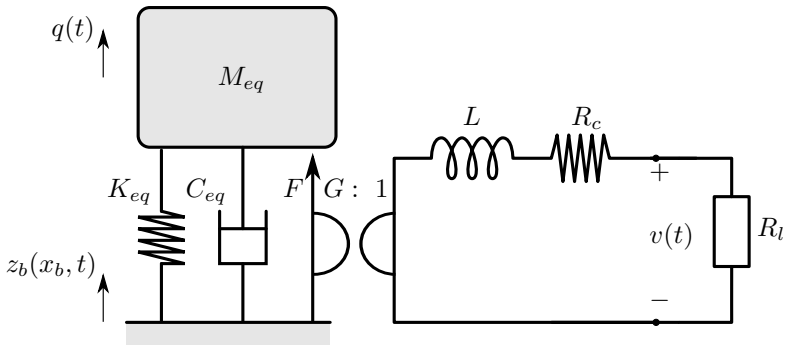

Figure 2: Lumped-parameter model of a magnetoelastic energy harvester.

previous equations allows us to calculate the amplitudes of displacement and voltage:

$$q_0(\overline{\omega}) = \frac{M_{eff}\overline{\omega}^2 z_0(x_b,\overline{\omega})/M_{eq}}{2\iota\overline{\omega}\zeta\omega + \omega^2 - \overline{\omega}^2 + \iota\overline{\omega}G^2/\left(M_{eq}\left(\iota\overline{\omega}L + (R_l + NR_c)\right)\right)} \tag{34}$$

$$i_0(\overline{\omega}) = \frac{\iota\overline{\omega}Gq_0(\overline{\omega})}{(\iota\overline{\omega}L + (R_l + NR_c))} \tag{35}$$

Equations (34) and (35) provide the response of the energy harverster under the base excitation z_0 acting at the frequency $\overline{\omega}$.

The derivation of the former expressions is based on the parameters β, γ and τ that relate the geometry and mechanical properties of the beam section with MsM to the substructure. These parameters facilitate the optimal harvester tuning procedure in the following sections.

2.2 Optimal design procedure

The performance of the device is limited to a narrow band around the resonance frequency, and then the power is drastically reduced if the excitation frequency deviates from resonance. The procedure for adjusting the resonant frequency of the harvester to the fundamental mode shape of the bridge follows the strategy described in [3].

The methodology adopted consists of: $i)$ the harvester tuning frequency is set to the optimum tuning frequency of the bridge ω_t [5]; and $ii)$ the damping coefficient C_{eq} is the same regardless of the bridge to which the harvester is tuned, allowing a comparable analysis of the collected energy [6]. The last condition is satisfied by defining the design parameter $r = K_{eq}M_{eq}$. All the above and the parameter γ allow determining the thickness and length of the substructure, h_s and L_s, and the tip mass M_t to adjust the harvester to the fundamental frequency of the bridge. Moreover, the proposed methodology considers the electric resistance and the number of turns of the pick-up coil to optimise the power generated $P(\overline{\omega})$.

The tuning procedure optimise the power dissipated by the load resistance under resonant conditions setting $\overline{\omega} = \omega_t$. The maximum amplitude of the harmonic base excitation is limited to $\ddot{z}_0(\overline{\omega}) = 3.5\,\text{m/s}^2$, which corresponds to the maximum acceleration level allowed on ballast railway bridges [7]. The harvester must withstand the stress in the substructure under this load, ensuring $\sigma_x(x) \leq \sigma_y$, where σ_y is the yield stress or the tensile strength. Several analyses have shown that the cross section in which the maximum stress is reached is found at $x = L_p$ ($\beta \leq 1$), which is located in the section of the substructure without MsM closest to the fixed end.

Additive manufacturing is selected for the substructure. The printing volume of a 3D printer limits the maximum length of the substructure. The maximum length of the substructure is constrained to $L_{s,max} = 0.3\,\text{m}$, which would be valid for most commercial 3D printers.

Then, the optimisation problem is defined as follows:

$$\begin{aligned} &\underset{r,\gamma,N,R_c}{\text{maximise}} \quad |P(\omega_t)| \\ &\text{subject to} \quad \sigma_x(L_p) \leq \sigma_y, \quad L_s \leq L_{s,max} \end{aligned}$$

The optimal solution is obtained using a genetic algorithm that starts to tune random individuals given by r, γ, N and R_c to the fundamental frequency of the bridge. Then, the optimal load resistance is calculated at the resonance frequency of the system, and the output power is evaluated if the constraints of the problem are satisfied. This process is repeated in subsequent generations to find the optimal design of the harvester.

3 Case study

In this section, energy harvesting on a High-Speed railway bridge is analysed using experimental records. In July and September 2022, the authors performed an experimental program on a HSL bridge crossing the Tirteafuera river including the identification of the bridge modal parameters and the recording of vibration levels under operational conditions. This bridge was a single simply-supported span concrete bridge with three tracks (see Figure 3). The deck was composed of a $18\,\text{m} \times 20.6\,\text{m}$ (length$\times$width) concrete slab resting on ten prestressed concrete girders. The slab carried two ballasted tracks with UIC gauge ($1.435\,\text{m}$) for high-speed trains and one ballasted track with Iberian gauge ($1.668\,\text{m}$) for conventional traffic.

The tests were carried out in two stages. First, the bridge response due to railway traffic was measured with a laser vibrometer. This allowed for the identification of the optimal tuning frequency according to [5]. Next, the proposed procedure was validated experimentally using a comprehensive experimental campaign consisting of the measurement of the bridge response from both ambient and forced vibrations. Figure 4 shows the sensors layout on the deck. The results of the second test include the identification of the bridge modal properties and the energy harvested under operating conditions.

Figure 3: HSL bridge under study: general view (38°43'33.06"N 4°5'20.05"W).

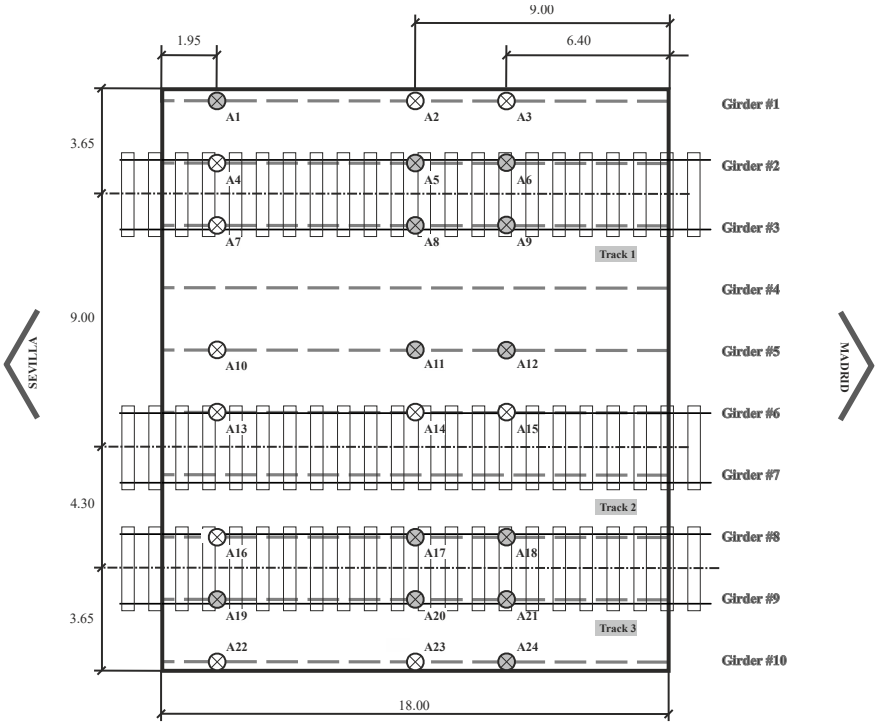

Figure 4: Sensor layout.

The results of the experimental program provided an optimal tuning frequency $f_t = 9.3\,\text{Hz}$ to which the harvester is designed. This frequency is introduced in the optimal design procedure detailed in the previous section. The energy harvester consists of a Metglas2605SC magnetoelastic layer $50\,\text{mm} \times 30\,\text{mm} \times 0.2\,\text{mm}$ glued to a PAHT CF15 substructure. Table 1 shows the results of the optimal design procedure for a device tuned to $f_t = 9.3\,\text{Hz}$.

Finally, the energy harvested due to a RENFE S102 in duplex configuration travelling on track 3 at $211.4\,\text{km/h}$ was estimated from the vibration of the bridge at the point $A23$. The bridge acceleration and voltage on the load resistance are shown in Figure 5. An overall analysis shows that the response is highly amplified and exhibits resonant behaviour. The energy harvested by the device is estimated to be $E = 5.28\,\text{mJ}$.

Table 1: Optimal design parameters

Tuning frequency	L_s[mm]	h_s[mm]	M_t[kg]	$R_l[\Omega]$	N[turns]	$R_c[\Omega]$
$f_t = 9.3\,\text{Hz}$	100.3	1.2	0.076	2219.5	1000	0.001

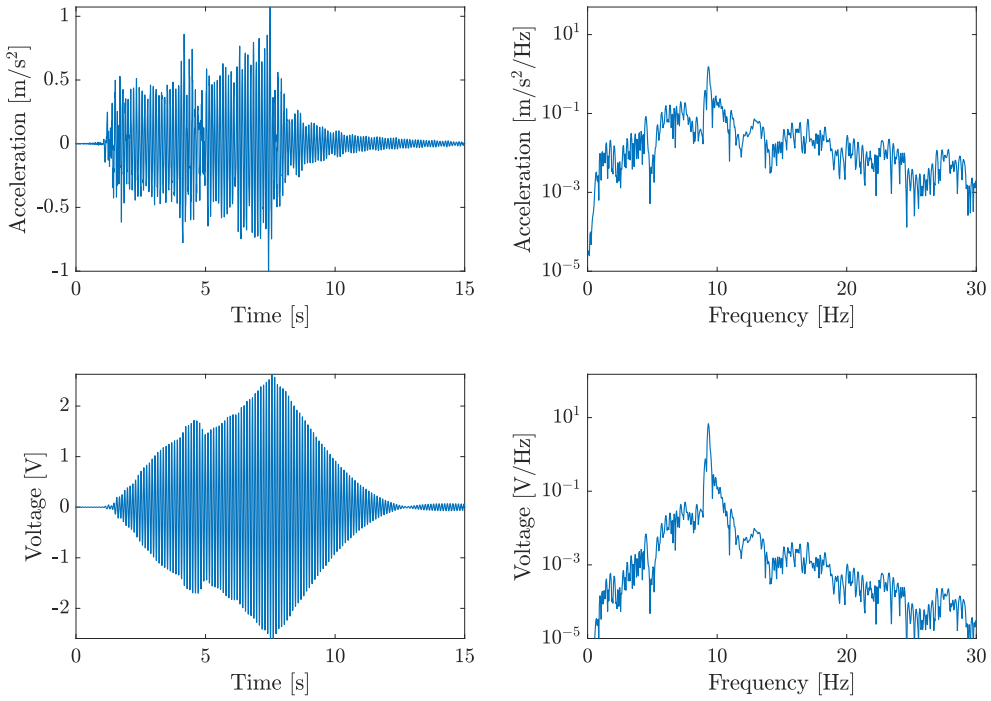

Figure 5: Bridge acceleration and voltage at point $A23$ induced by Renfe S102-Duplex train circulating on track 3 at $V = 211.4\,\text{km/h}$.

4 Conclusions

The work presented in this research is within the objectives of developing autonomous monitoring systems. In this way, it will be possible to reduce maintenance costs and extend the useful life of the railway infrastructure. The aim of this research is the analysis of the performance of magnetoelastic energy harvesting on railway bridges. This research proposes an analytical model that allows an optimal design of a harvester device for each railway bridge such that maximum power is obtained. The conclusions drawn from the experimental case study show that the harvested energy in a train passage over the bridge under study by a device tuned to optimal tuning frequency $9.3\,\text{Hz}$ could be $E = 5.28\,\text{mJ}$. Although the available power is small for a single train, this energy source can be used in intermittent storage and measurement operations. The amount of energy can be increased using several harvesters according to the output required power of a monitoring system. Then, the results of this analysis are expected to be helpful for energy harvesting applications on railway bridges to feed low power consumption devices, nodes, and sensors of monitoring systems in remote areas, and

also for the development of harvesters as direct structural health monitoring devices.

Acknowledgements

The authors would like to acknowledge the financial support provided by the Spanish Ministry of Science, Innovation and Universities under the research project PID2019-109622RB; Spanish Ministry of Science and Innovation under the research project PID2022-138674OB; PROYEXCEL_00659 funded by Regional Ministry of Economic Transformation, Industry, Knowledge and Universities of Andalusia; Generalitat Valenciana under the research project AICO/2021/200, and the Andalusian Scientific Computing Centre (CICA).

References

[1] T. Yildirim, M.H. Ghayesh, W. Li, G. Alici, A review on performance enhancement techniques for ambient vibration energy harvesters, Renewable and Sustainable Energy Reviews 71 (2017) 435–449.

[2] L. Wang, F.G. Yuan, Vibration energy harvesting by magnetostrictive material, Smart Materials and Structures 17-4 (2008).

[3] J.C. Cámara-Molina, E. Moliner, M.D. Martínez-Rodrigo, D.P. Connolly, D. Yurchenko, P. Galvín, A. Romero, 3D printed energy harvesters for railway bridges-design optimisation, Mechanical Systems and Signal Processing 190 (2023) 110133.

[4] IEEE Standard on Magnetostrictive Materials: Piezomagnetic Nomenclature, Standard (1990).

[5] J.C. Cámara-Molina, A. Romero, E. Moliner, D.P Connolly, M.D. Martínez-Rodrigo, D. Yurchenko, P. Galvín, Design, tuning and in-field validation of energy harvesters for railway bridges, Mechanical Systems and Signal Processing 208 (2024).

[6] A. Romero, J.C. Cámara-Molina, E. Moliner, P. Galvín, M.D Martínez-Rodrigo, Energy harvesting analysis in railway bridges: An approach based on modal decomposition, Mechanical Systems and Signal Processing 160 (2021).

[7] CEN, EN 1991-2, Eurocode 1: Actions on Structures - Part 2: Traffic loads on bridges, European Committee for Standardization, Brussels, 2002.